This paper appears in the Proceedings of IEEE International Conference on Robotics and Automation, Xi'an, China, 2021.

A Low-cost Intrinsically Safe Mechanism for Physical Distancing Between Clinicians and Patients

Abed Soleymani, Ali Torabi, Mahdi Tavakoli

***Abstract*—During the COVID-19 pandemic, due to the unprecedented workload and cross-infection hazard, the healthcare workers' lives are under a significant threat. However, minimizing the duration and frequency of close clinician-to-patient contacts using simple technologies that enable physical distancing could reduce the risk of spreading the disease. In this context, this paper presents the conceptual design and preliminary assessment of a low-cost and intrinsically safe remote service delivery platform that can assist clinicians in doing various tasks at a safe distance from patients. This mechanism is capable of manipulating objects in three-dimensional Cartesian space and can be adapted to handling a wide variety of medical devices. Moreover, its passive weight-compensating design provides the mechanism with high maneuverability, enhanced dynamic manipulability, and better force feedback quality. The advantages and effectiveness of the proposed mechanism are demonstrated through experiments. In the experiment, an ultrasound probe is mounted at the end effector of the device to perform an imaging task from a safe distance. Due to the existence of the force feedback, the user could remotely manipulate the ultrasound probe for having a successful vertical and pivot scanning to get high-quality images with a low physical and mental demand.**

I. Introduction

The COronaVIrus Disease 2019 (COVID-19) outbreak is one of the most unprecedented challenges that modern human life has encountered in the recent century. The disease's uncontrolled spread, high contagiousness, and relatively high mortality have put a sudden and massive burden on healthcare providers and staff around the world in terms of extra workload as well as endangering their lives [1].

Medical workers, due to their frequent and close contact with COVID-19 patients bear a higher risk of contracting the disease. For instance, in Italy, about 20% of healthcare workers were infected with COVID-19 [2]. Precautions such as using personal protective equipment (PPE) and physical distancing will dramatically reduce the spread and severity of the disease. Frontline healthcare workers are compelled to strictly follow self-protection mandates including a strict PPE level that reduces their comfort, efficiency, and accuracy [1]. Overreliance on PPE in fighting against COVID-19 could lead to a disaster in case of PPE shortage.

* This research was supported by the Canada Foundation for Innovation (CFI), the Government of Alberta, the Natural Sciences and Engineering Research Council (NSERC) of Canada, the Canadian Institutes of Health Research (CIHR), and the Alberta Economic Development, Trade and Tourism Ministry's grant to Centre for Autonomous Systems in Strengthening Future Communities.

A. Soleymani, A. Torabi, and M. Tavakoli are with the Department of Electrical and Computer Engineering, University of Alberta, Edmonton, AB, Canada. {zsoleymani, ali.torabi, mahdi.tavakoli}@ualberta.ca

Maintaining physical distancing in the clinic (i.e., remote health service delivery) by reducing the need for person-to-person contact protects healthcare staff from COVID-19 and other contagious diseases and decreases the required PPE level and PPE consumption. Moving from manually performing clinical tasks at a close distance to teleoperating these tasks from a safe distance seems to be a reasonable and promising direction.

Telerobotic systems have a long history of use in healthcare settings. For instance, telerobotic systems for minimally invasive surgery have been commercially available for the past 20 years. The daVinci Surgical Robot made by Intuitive has obtained widespread adoption in hospitals all over the world. Generally, robotic-assisted medical devices are superior to manually controlled devices in terms of target reached, the precision of movement, and reliability [3]. Robotic mechanisms can help healthcare staff during the COVID-19 pandemic to fulfill a wide variety of tasks from a safe distance in the same room [4]. For instance, [5] incorporates a telerobotic system composed of a wearable initial motion capture device and a dual-arm collaborative robot to remotely perform a variety of healthcare service delivery tasks ranging from a simple drug delivery to remote operation of the medical instruments in ICU room. Furthermore, robotics systems can perform more sophisticated medical tasks including remote ultrasound imaging to deliver a higher precision, dexterity, and repeatability of the operation to the user. For example, [6] developed a robot-assisted tele-echography for scanning moving organs such as heart and chest during their natural movements, i.e., breathing or beating. Last but not least, in [7], the user controls a robotic arm with a joystick to manipulate a video laryngoscope in the mouth of the patient, to open the airways, and insert the tracheal tube to remotely complete the intubation task, which is a frequently done during COVID-19 pandemic in ICU rooms and emergencies.

However, the above-mentioned approaches have some fatal drawbacks. Using active (i.e., powered) mechanisms such as previously mentioned devices, involves complexity, cost, and a long regulatory approval process. In contrast, there is an urgent need for a remote health service delivery platform to decrease the exposure risk of healthcare staff to the COVID-19 at the present time. Active control mechanisms (e.g., a joystick) might be unfamiliar for clinical users. In this busy time, there is a little chance for medical staff to learn a new way of doing their previous routines.

On the other hand, it is possible to design passive, human-powered, intrinsically safe mechanical solutions for health ser-

vice delivery from a safe distance. These mechanisms benefit from simple-to-use and low manufacturing cost features and can get the regulatory approval in a relatively easy procedure [8].

This paper's objective is to perform the design, construction, and preliminary assessment of a novel passive health service delivery device that protects clinical staff and reduces human-to-human contact by facilitating manual teleoperation of fine-positioning and delicate manipulation tasks. These tasks include patient examination (e.g., auscultation), swab taking, adjustment of ICU monitors, dials and touch screens, oxygenation, and ultrasound scanning. Another advantage of the proposed device is that because it is fully mechanical and requires no powerup or calibration routine, it can be quickly deployed in emergencies similar to most conventional tools. Based on the proposed device's prospects of fast regulatory approval, low price, and intrinsic safety due to being under human power and control, it is appealing for use during the COVID-19 pandemic and is bound to find more and more creative applications in hospitals once clinicians see it in action. Last but not least, this mechanism, based on its intuitive design, helps its users to accomplish tasks using their familiar techniques.

The outline of the paper is organized as follows: In Section II, general approach of the mechanical design and kinematics analysis will be discussed. In Section III, kinematics optimization of the device will be presented. In Section IV, dynamics optimization of the device with the aim of enhancing the user interaction will be investigated. In Section V, the prototype construction and pre-clinical evaluation will be explained. Concluding remarks are provided in Section VI.

II. Design Specifications

A good design of the mechanism's structure plays a vital role in its overall efficacy in doing assigned tasks. A good design of the proposed mechanism for above-listed clinical tasks should features: backdrivability, a singularity-free workspace, a unique solution for the inverse kinematics, and a large workspace. In this section, all of the above-mentioned specifications will be addressed in the design procedure.

A. Mechanism Design

For almost all clinical tasks, at least three degrees of freedom (DoF) are required for the end effector so that the user can freely manipulate the position of the medical device in the 3D space. We decoupled the tool's Cartesian motion into horizontal (xy) and vertical (z) movements. The horizontal motion can easily be achieved by a 2-DoF linear motion stage. To achieve position control in the z direction, the end effector should follow a straight vertical line and be remotely controlled with a similar vertical motion at the user handle. Inspired by [9], we used the Grasshopper approximate straight line mechanism. This backdrivable mechanism enjoys an approximately perfect vertical motion with the input and output displacement in the same direction. This mechanism is illustrated in Fig. 1 in which all of the link lengths are

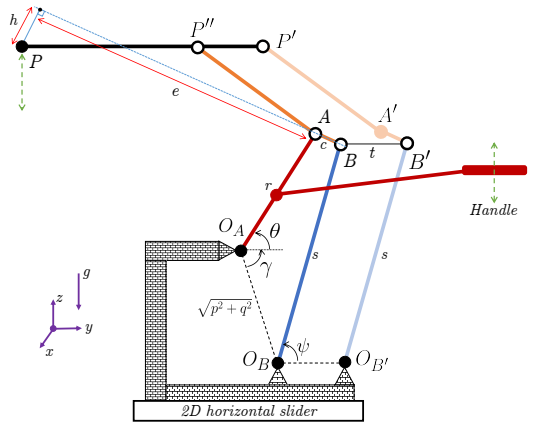

Fig. 1. Schematic view of the vertical motion mechanism adopted from Grasshopper mechanism and its parameters.

constant, and the user could manipulate the end effector P in the z direction by changing the angle θ with the motion of lever $O_A A$.

B. Kinematics

Due to the kinematic of the four-bar linkage mechanism, the position of the end effector P can be written as an explicit nonlinear function of input angle θ as defined in Fig. 1. Detailed derivation of the forward kinematics is provided in Appendix A.

Generally speaking, closed chain mechanisms suffer from singular configurations at so called bifurcation points, where the Jacobian matrix has rank deficiency and these points connect parallelogram and anti-parallelogram shapes of the four-bar linkage together. Because of the confined motion of the input angle θ in this particular mechanism, the four-bar-mechanism will not reach kinematic bifurcation points. As a result, there is a unique solution for the inverse kinematic problem for any value of θ in the workspace. The horizontal orientation of the end effector P should be preserved all the time with the variation of input angle θ to create a level medium for mounting a variety of appliances. This feature can be achieved by incorporating parallel auxiliary links for BO_B and BP'' (see Fig. 1). With the addition of these links, the line PP' is horizontal all the time with the variation of θ.

C. Workspace Evaluation

Due to the joint and geometry limitations, robots impose constraints on the end effector movements. One of the numerous standard techniques for quantifying the workspace efficiency is the kinematic manipulability measure [10]. The kinematic manipulability measure of the proposed mechanism at the input angle θ is defined as $w = \sqrt{\det\left(J(\theta)J^T(\theta)\right)}$, where $J(\theta)$ is the Jacobian matrix of the robot manipulator.

Intuitively, kinematic manipulability measure w represents the mapping between input velocity $\dot{\theta}$ to the output velocity $\dot{P}$ (for simplicity, the position of point P is shown as P, and the same applies to other points shown in Fig. 1). Higher kinematic manipulability measures of the device determine

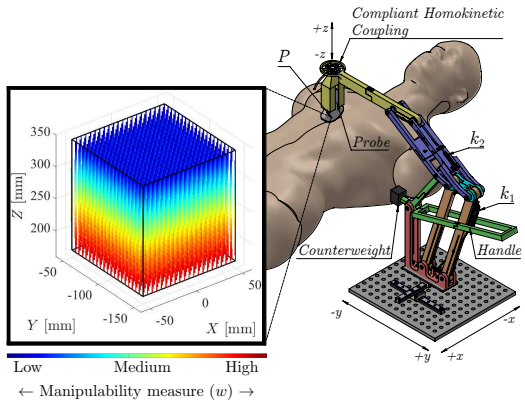

Fig. 2. Real-size schematic view of the mechanism in comparison with an averaged size human, and the working space of the end effector P with the kinematic manipulability measure (w) visualization.

better postures and better points in its workspace in terms of dexterity and maneuverability. These configurations are called optimal postures and optimal working positions.

Fig. 2 illustrates the kinematic manipulability measure for the proposed mechanism in its workspace based on the optimal results which will be discussed in Section III. It shows that kinematic manipulability measure is at its maximum value in the vicinity of the patient where the device is operating. It means that the device has the best maneuverability and enhanced dexterity when it is operating near the patient compared with other configurations of the device. Additionally, note that due to the safe margin from bifurcation, the workspace is singularity free.

D. Compliant Interaction with the Patient's Body

In tasks such as sonography and oxygenation, it is necessary to have a compliant interaction at the contact point of the end effector with the patient's body. This feature could be passively achieved by implementing a compliant homokinetic coupling between the end effector P and the medical device (see Fig. 2 and Fig. 5). This solution improves the maintenance and cleanliness of this platform as two important requirements of medical devices and precision instruments [11].

III. Kinematics Optimization

With the exceptionally designed kinematic features explained in Section II, the proposed mechanism has the potential to be further optimized to enhance its user interaction quality in terms of precise positioning and lower cognitive load on the user while performing the task. Kinematics optimization can be done based on two criteria: exact vertical motion of the end effector P in the workspace of the device, and linear mapping between the handle velocity and the vertical velocity of the end effector P.

The Cartesian position of the end effector could be expressed as a non-linear function f of the input parameter θ as

$$P = f(\theta) \Rightarrow v_P = \frac{dP}{dt} = \frac{\partial f(\theta)}{\partial \theta}\dot{\theta} = J(\theta)\dot{\theta} \qquad (1)$$

where v_P is the linear velocity of the end effector and $J(\theta) = \frac{\partial f(\theta)}{\partial \theta}$ is the Jacobian matrix of the manipulator. For the kinematics, two criteria could be adopted for the optimization procedure. The first criterion is preserving vertical motion of the end effector P (i.e., minimum displacement in the y direction) when the user moves the handle to adjust the vertical position. The second one is achieving the maximum linearity of the matrix J in correspondence to the mapping between angular velocity $\dot{\theta}$ to vertical velocity $\dot{P}_z$ (i.e., J must be as θ-independent as possible). In other words, with the constant velocity of the handle, the user should get constant vertical velocity at the end-point P (note that $\dot{P}_H = L_H\dot{\theta}$ where $\dot{P}_H$ is the linear velocity of the handle and the constant L_H is the length of the handle). Therefore, a cost function for the optimization is defined as

$$C = \left[w_1\sigma^2_{P_y} + w_2\sigma^2_{\dot{P}_z}\right]_\Theta \qquad (2)$$

where w_1 and w_2 are weight factors, and Θ is a uniformly ascending set of input angle θ from θ_0 to θ_1. The four-bar linkage in the input range of $[\theta_0, \theta_1]$ does not pass any bifurcation point and has a approximate straight line behavior at the end-point P. Moreover, σ_{P_y} is the standard deviation of the end effector P movements in the y direction when θ varies from θ_0 to θ_1. The smaller value of $\sigma^2_{P_y}$ delivers pure vertical motion of point P, and as a result, better control of the end effector during the operation. Finally, $\sigma_{\dot{P}_z}$ is the standard deviation of the vertical linear velocity of the point P during the transition of angle θ from θ_0 to θ_1 with the constant angular velocity. Minimizing $\sigma_{\dot{P}_z}$ based on the uniformly ascending input θ, converges the velocity of the end effector P in the vertical direction to a constant value. Therefore, optimizing the Grasshopper kinematic parameters subject to cost function C benefits the platform's total functionality. The initial values for the parameters were selected as the kinematic values of a common Grasshopper mechanism with an acceptable vertical straight motion of end effector P. After the convergence of the optimization algorithm with weight parameters $w_1 = 2$ and $w_2 = 1$, there was a considerable improvement in the kinematical behavior of the system. As illustrated in Fig. 3, minimization of the cost function C decreases the value of $\sigma^2_{P_y}$ which reshapes the P_z vs. P_y profile to a vertical line. Moreover, the optimization process reduces the value of $\sigma^2_{\dot{P}_z}$ during the constant movement of the handle, and as a result, the $\dot{P}_z/\dot{P}_H$ profile asymptotes to a horizontal line that means the linear mapping between input and output velocities. Moreover, the ration of $\dot{P}_z/\dot{P}_H$ could be adjusted by tuning the handle length to achieve different force/displacement transmission ratio which has a great impact on the user comfort and task accuracy. Optimization results in millimeter are: $r = 215.8$, $c = 47$, $q = 73.9$, $e = 213.5$, $s = 349.6$, $p = 57$, $h = 57$, and $t = 80$.

IV. Dynamics Optimization

A robotic system, especially when it is interacting with a human, needs to possess certain dynamical features such as

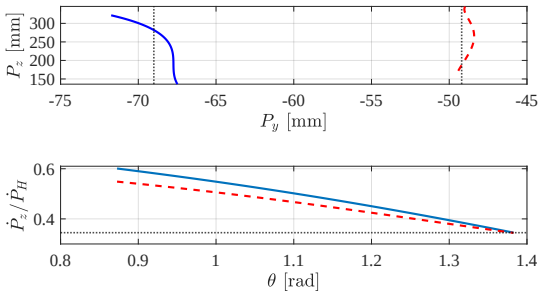

Fig. 3. Kinematics optimization results based on the cost function C for initial configuration (solid blue line), optimized configuration (dashed red line), and the ideal line (dotted black line).

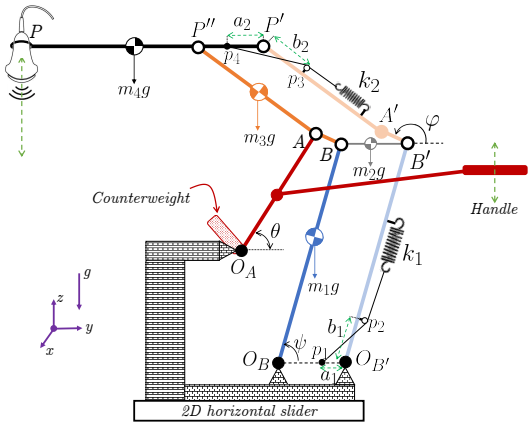

Fig. 4. The schematic design of the whole mechanism based on parallelogram and the combination of counter weight and zero-rest-length spring based balancing approaches.

fully or partially compensated weight, truthful force transmission to the user, minimum required effort from the user, and low apparent inertia. The journey of the dynamics optimization based on the described objectives starts with the concept of energy conservation.

Energy conservation is about maximizing the efficiency of energy flow in mechanical systems. This not only reduces the user's energy consumption (and as a result, decreases the user's effort), but also results in the enhancement of system functionalities, such as a reduction in the overall weight or improving the quality of force transmission through the system from the end effector to the user's hand [12]. In human-robot interaction applications, while it is impossible to have a perfect force transmission, it has been proven that better force transmission quality yields a better user performance and enhances the users' perception while performing the task. Therefore, high fidelity force feedback decreases users' mental load in sophisticated tasks [13].

Statically balanced systems are good examples of mechanical systems that conserve energy via weight compensation in almost all of their workspace using totally passive approaches. Also, it can be proven that weight compensation provides an improved dynamic manipulability of the system for the user and reduces the apparent inertia of the device (see Appendix B). Intuitively, dynamic manipulability in the proposed mechanism determines the strength of the mapping function between the input force at the user's handle to the output force at the end effector and vise versa. For the proposed mechanism shown in Fig. 1, which is a single input (θ) and single output (P) mechanism, dynamic manipulability characterization is done by studying the impulse response of the system to a unit normed force at the input of the system. This could be interpreted that enhanced dynamic manipulability results in an improved force feedback to the user through the system.

Since the energy conservation approach is based on the static state of the system, the kinetic energy must be zero. Also, Potential Energy $\mathcal{P}$ should be constant in all configurations (i.e., $\frac{\partial \mathcal{P}}{\partial \theta} \equiv 0$). Additionally, based on the superposition law, one can statically balance one degree of freedom while freezing other ones and finally, consider all of the balancers together [12].

The weight compensation mechanism of the proposed device has three components: spring-based weight compensation of the upper parallelogram with the stiffness of k_2, spring-based weight compensation of the lower parallelogram with the stiffness of k_1, and weight compensation of the handle using a counterweight. According to [14] and parameters shown in Fig. 4, spring-based weight compensation of the parallelogram $BB'P'P''$ could be passively achieved by incorporating a zero-free-length spring (see [12]) with the stiffness of k_2 at link $B'P'$. The potential energy of the upper parallelogram $BB'P'P''$ while freezing another parts of the mechanism could be expressed as $\mathcal{P}_2 = -m_4 gl\cos(\varphi) - 2 \times m_3 g\frac{l}{2}\cos(\varphi) + \frac{k_2}{2}(x - x_0)^2$ where $l = |B'P'|$, and the mass of each link is equally distributed. Incorporating zero-free-length spring results $x_0 = 0$. Based on the cosine law, it holds that $x^2 = a_2^2 + b_2^2 + 2a_2b_2\cos(\varphi)$. Substituting these results into (IV) yields $\mathcal{P}_2 = -(m_3 + m_4)gl\cos(\varphi) + \frac{k_2}{2}\left(a_2^2 + b_2^2 + 2a_2b_2\cos(\varphi)\right)$. To statically balance this part of the system, the potential energy of the upper parallelogram ($\mathcal{P}_2$) should be constant for all of the input angle θ in the workspace. Consequently

$$\frac{\partial \mathcal{P}_2}{\partial \theta} = (m_3 + m_4)gl\sin(\varphi) - k_2a_2b_2\sin(\varphi) \equiv 0$$

which for $\theta \neq 0$ results in

$$k_2 = \frac{(m_3 + m_4)gl}{a_2b_2} \tag{3}$$

The parameter k_2 is completely independent of the variation of angle θ. This means that the weight compensation is achieved for all configuration of the upper parallelogram. Similarly, for the lower parallelogram $O_BO_{B'}B'B$, pure weight compensation could be achieved if

$$k_1 = \frac{(m_1 + m_2 + 2m_3 + m_4)gs}{a_1b_1} \tag{4}$$

where according to Fig. 1, $s = |O'_BB'|$. Weight compensation

for the handle is accomplished by attaching an appropriate counterweight at the other side of the lever. Based on the superposition law, the whole mechanism is statically balanced when three above-mentioned components are incorporated at the same time. The schematic design of the entire mechanism, based on the combination of counterweight and zero-rest-length spring-based balancing approaches, is illustrated in Fig. 4. The overall performance of the prototype are investigated in Section V.

V. Pre-clinical Assessment

In this section, a pre-clinical assessment will be done to test all of the design criteria mentioned earlier in practice. While numerous applications could be imagined for this type of device, we focused on the relatively sophisticated task of ultrasound scanning. We picked this task because COVID-19 patients with underlying conditions are at a higher risk and one of the ways to assess patients background condition is sonography. The procedure of the evaluation is provided as follows.

A. Prototype

A prototype of the proposed mechanism with the optimized kinematics parameters was built via a 3D printer to perform some clinical experiment as a proof of concept. The fabricated mechanism is smaller than what would afford a 2m physical distance. However, it is possible to elongate the handle or the link $P''P$ for more distance or scale up the entire mechanism's lengths. Before delving into the device analysis, some challenges should be dealt with to make the setup ready for the ultrasound scanning task.

1) Mechanism Tuning: The solution explained in the paper is supposed to provide the same set of weight compensation springs to a variety of tools attached at the end effector of the device by using adjustable attachment points p_i $(i = 1, 2, 3, 4)$ (see Fig. 4). In other words, by changing the tool at the end effector P of the device the value of m_4 changes, and as a result, k_1 and k_2 should be modified based on (3) and (4) to have a weight compensation for the new situation. However, by changing the attachment points p_i $(i = 1, 2, 3, 4)$, the user can adjust values of a_1, b_1, a_2, and b_2 to cancel the variation of m_4 in (3) and (4) to keep the values of k_1 and k_2 constant. As shown in Fig. 2, this could be achieved by generating a fine grid of evenly-spaced slots on links $O_BO'_B, B'O'_B, B'P'$, and $P'P''$ and inserting tiny pins into these holes to hold cable endings (p_1 and p_4) and guidance points (p_2 and p_3).

2) Probe Manipulation: The mechanism introduced so far provides means of vertical scanning of the ultrasound probe, benefiting the user with the positioning of the probe on the intended location on the patient's skin and exerting appropriate contact force to it. Moreover, due to the mechanical advantage provided by the device, the exerted force on the handle will be magnified at the end effector P. This feature alleviates orthopedic strain and injury while performing ultrasound scanning procedure. Several publications have highlighted the strain on sonographers holding the probe for a long time in an uncomfortable position [15], [16]

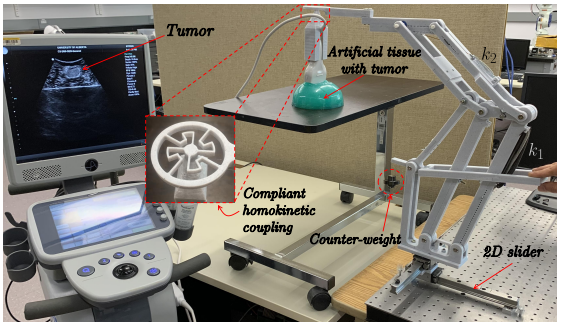

Fig. 5. The 3D printer experimental setup for the proof of concept of the usability of the proposed mechanism in the ultrasound imaging task on a phantom tissue.

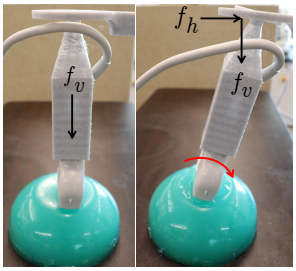

(a) Vertical scanning (left) and pivot scanning (right).

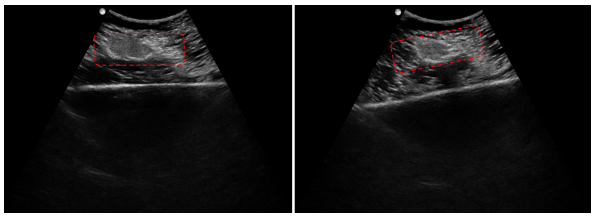

(b) Vertical scanning ultrasound image (left) and pivot scanning ultrasound image (right) on the same tissue.

Fig. 6. Vertical scanning and pivot scanning. Pivot scanning is the result of horizontal displacement of the device (f_h) maintaining the vertical force f_v.

To get a wider and higher-quality view of the target organ, pivot scanning must be done alongside the vertical scanning [17]. In pivot scanning, the transducer is slightly swept, pivoting on the point of interest by changing the pitch and yaw orientation of the probe in a fixed contact point. This feature could be passively achieved by implementing a compliant homokinetic coupling between end effector P and ultrasound probe (see Fig. 5). The pitch and yaw orientation of the probe could be controlled by the displacement in xy plane using the horizontal slider when the probe reaches the intended point, gaining appropriate contact force via vertical movement (see Fig. 6).

B. Experiment Protocol

In the experiment, the ultrasound probe is connected to the Ultrasonix Touch ultrasound scanner (Analogic Corp, Peabody, MA, USA) to obtain the image from a biomimetic

tissue with a built-in simulated tumour. The artificial tissue used in experiments is a phantom tissue sample, created from the plastisol (M-F Manufacturing Co, Fort Worth, USA).

In experiments, individuals who had little prior experience of manual ultrasound scanning were asked to perform the imaging task in three steps. The experiments were approved by the University of Alberta Research Ethics and Management Online under study ID Pro00070096. In the first step, each participant was asked to manipulate the platform in the free space and test the ultrasound imaging process using the device in a short training interval.

In the second stage, participants were allowed to perform the ultrasound scanning task to get a clear and diagnosable image of the tumor in three trials performed at three different contact points with the tissue. External forces such as those caused by respiration were artificially introduced by the examiner through periodically squeezing the tissue sides. Due to the various contact points, participants unconsciously used all of the scanning techniques, including exerting variable vertical force and pivot scanning, to get a clear and diagnosable image.

Finally, in the third step, participants were requested to fill the NASA Task Load Index (NASA-TLX) assessment form to assess the perceived overall efficacy of the proposed device. The performance assessment protocol was based on the five subjective subscales: mental demand, physical demand, performance, effort, and frustration; all of them rating from 1 (very low) to 20 (very high) [18].

C. Results

Five participants performed the ultrasound imaging process using the device based on the above-mentioned protocols. All of them managed to perform vertical and pivot scanning over the phantom tissue and thanks to the wight compensation mechanism, they had a real-time and pure haptic feedback to control the contact force all the time to get a high-quality image at the presence of the external forces. Moreover, all of the participants were satisfied with accurately performing their intended scanning trajectory, and had a successful experience in scanning the artificial tumor in all of three intervals in terms of clarity and diagnosability.

The statistical results of the NASA-TLX subjective assessment tool for all participants and all trials are presented in Fig. 7. Based on the performance results, all of participants had a good experience with the usability and performance of the device in a relatively complicated ultrasound scanning task.

Moreover, participants were unanimous about the low required physical demand, and generally speaking, the small amount of required effort in accomplishing the task. It can be attributed to the gravity compensation in the device and the comfortable posture of the shoulder joint during ultrasound imaging with this device. The main advantage of this achievement is that the strain on the user's shoulder and neck dramatically decreases while performing the task. This pressure is the main contributing factor in widely reported injury and chronic pains in the shoulder and neck joints and muscles of ultrasound technicians.

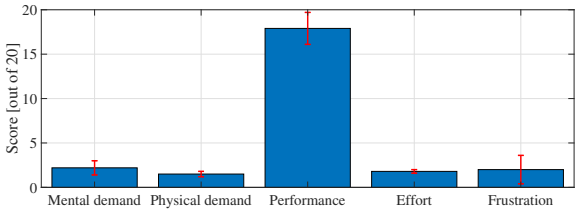

Fig. 7. NASA-TLX results' diagram for five subjective subscales for five participants. Mental demand: 2.2 ± 0.8, physical demand: 1.5 ± 0.3, performance: 17.9 ± 1.8, effort: 1.8 ± 0.2, and frustration: 2.0 ± 1.6

Finally, based on the platform's intuitive design, users were not forced to do the task in a different way from their previous experiences. In other words, participants did not feel frustrated or confused about the platform's working principle and managed to work with the device with a little mental demand. As a result, they quickly acquired experience in working with the device.

VI. Discussion and Conclusion

A remote healthcare service delivery system with multiple applications was proposed in this paper. This device can provide a simple, safe and human-powered platform for reaching, sensing and manipulation to deliver a variety of healthcare services from a safe distance. It has the potential to protect critical care and other hospital staff from COVID-19 or other contagious diseases when they care for patients. Thanks to the safe adjustable distance provided by this device, clinical staff will be less required to follow a strict PPE level, thus having more comfort and less physical pressure during their working hours. Overall, there are going to be significant impacts in terms of decreasing the cross-infection risk between hospital staff and patients and increasing the quality of care provided to patients. Additionally, this robotic platform with such an intuitive operation, gravity compensation, and end effector compliance can assist healthcare staff by providing physical convenience without imposing a high cognitive load for performing operations.

A user study was done based on an ultrasound scanning task in which the NASA-TLX subjective assessment method was done on five participants. Based on the acquired results, the proposed device has demonstrated excellent performance in ultrasound scanning tasks and helped the users to get high-quality images of the artificial tumor.

Appendix

A. Forward Kinematic of the Four-bar Linkage

The forward kinematic of the four-bar linkage presented in Fig. 1 can be expressed in detail as follows

$$P = f(\theta) = \begin{bmatrix} x \\ y + y_{O_A} + [e(y_{O_A} - y_{O_B}) + h(z_{O_B} - z_{O_A})]/c \\ z_{O_A} + [e(z_{O_A} - z_{O_B}) + h(y_{O_B} - y_{O_A})]/c \end{bmatrix} \tag{A.1}$$

where x and y are the horizontal locations of the base in the horizontal motion slider [19]. Moreover, O_A =

$\begin{bmatrix} x & y+u & v \end{bmatrix}^T, O_B = \begin{bmatrix} x & y+u+p & v+q \end{bmatrix}^T$, $y_{O_A} = y+u+r\cos(\theta)$, $z_{O_A} = v+r\sin(\theta)$, $y_{O_B} = y+u+p+s\cos(\psi)$, and $z_{O_B} = v+q+s\sin(\psi)$. Because of the kinematic loop constraint in the four-bar linkage, angle ψ depends on the input angle θ and can be expressed as

$$\psi = \tan^{-1}\left(\frac{\beta}{\alpha}\right) + \cos^{-1}\left(\frac{\phi}{\sqrt{\alpha^2+\beta^2}}\right) - \gamma \qquad \text{(A.2)}$$

where $\alpha = 2s\sqrt{p^2+q^2} - 2rs\cos(\theta+\gamma)$, $\beta = -2rs\sin(\theta+\gamma)$, $\phi = c^2 - (p^2+q^2) - s^2 - r^2 + 2r\sqrt{p^2+q^2}\cos(\theta+\gamma)$, and $\gamma = \tan^{-1}(q/p)$. Therefore, angle ψ and forward kinematics expressed in (A.1) can be written as an explicit function of input angle θ as expressed in (A.2). As a result, the non-linear forward kinematics function f is parametrized just by the single input θ.

Because of the confined motion of the input angle θ in the proposed mechanism, the four-bar linkage will not reach bifurcation points. As a result, there is a unique solution for ψ in (A.2) for any value of θ in the workspace of the device. In the other words, the inverse kinematics has a unique solution in all of the workspace of the proposed mechanism.

B. Gravity Compensation and the Dynamic Manipulability

According to (1)

$$a_P = \frac{dv_P}{dt} = J\ddot{\theta} + \dot{J}\dot{\theta} \qquad \text{(A.3)}$$

where a_P is the linear acceleration of the end effector P. The dynamics equation of a robot manipulator could be expressed as follow

$$M(\theta)\ddot{\theta} + C(\theta,\dot{\theta})\dot{\theta} + g(\theta) = \tau \qquad \text{(A.4)}$$

where $M(\theta)$ is the symmetric positive-definite inertia matrix, $C(\theta,\dot{\theta})$ is the vector containing the Coriolis and centripetal torques, $g(\theta)$ is the vector containing the gravitational torques, and τ is the required torque for manipulating the robot in the particular configuration based on the angle θ. Note that the static balancing condition yields $\dot{\theta} = 0$ and (A.3) and (A.4) simplify to $a_P = J\ddot{\theta}$ and $M(\theta)\ddot{\theta} + g(\theta) = \tau$ respectively. Defining $\hat{\tau} = \tau - g(\theta)$ yields

$$|\hat{\tau}| \leq \tau^{\max} - |g(\theta)| \qquad \text{(A.5)}$$

where $\tau^{\max}$ is the maximum driving torque of the joint O_A provided by the user's handle. Moreover, assume that $|a_P| \leq a_P^{\max}$ where $a_P^{\max}$ is the maximum linear acceleration that the user can provide at the end effector side by moving the handle. According to [20], the dynamic manipulability of the device is equal to

$$w_d = \sqrt{\det\left(\hat{J}(\hat{M}^T\hat{M})^{-1}\hat{J}^T\right)} \qquad \text{(A.6)}$$

where $\hat{M} = \text{diag}\left(1/[\tau^{\max} - |g_i(\theta)|]\right) M$ and $\hat{J} = \text{diag}\left(1/[a_{P_i}^{\max}]\right) J$. It's beyond dispute that decrease in the value of $|g(\theta)|$ in (A.5) will increase the amount of $\tau^{\max} - |g_i(\theta)|$ and as a result, the total norm of matrix $\hat{M}$ decreases (i.e., reduction in the apparent inertia), and finally, based on (A.6) the value of w_d increases. Needless to say that the best dynamic manipulability can be achieved when $g_i(\theta) \equiv 0$, i.e., when the weight of the mechanism is totally compensated.

REFERENCES

[1] B. Gates, "Responding to covid-19—a once-in-a-century pandemic?" *New England Journal of Medicine*, vol. 382, no. 18, pp. 1677–1679, 2020.

[2] T. Lancet, "Covid-19: protecting health-care workers," *Lancet (London, England)*, vol. 395, no. 10228, p. 922, 2020.

[3] G. Ciuti, R. Donlin, P. Valdastri, A. Arezzo, A. Menciassi, M. Morino, and P. Dario, "Robotic versus manual control in magnetic steering of an endoscopic capsule," *Endoscopy*, vol. 42, no. 02, pp. 148–152, 2010.

[4] M. Tavakoli, J. Carriere, and A. Torabi, "Robotics, smart wearable technologies, and autonomous intelligent systems for healthcare during the covid-19 pandemic: An analysis of the state of the art and future vision," *Advanced Intelligent Systems*, p. 2000071, 2020.

[5] G. Yang, H. Lv, Z. Zhang, L. Yang, J. Deng, S. You, J. Du, and H. Yang, "Keep healthcare workers safe: Application of teleoperated robot in isolation ward for covid-19 prevention and control," *Chinese Journal of Mechanical Engineering*, vol. 33, no. 1, pp. 1–4, 2020.

[6] M. Sharifi, H. Salarieh, S. Behzadipour, and M. Tavakoli, "Tele-echography of moving organs using an impedance-controlled telerobotic system," *Mechatronics*, vol. 45, pp. 60–70, 2017.

[7] T. Hemmerling, R. Taddei, M. Wehbe, C. Zaouter, S. Cyr, and J. Morse, "First robotic tracheal intubations in humans using the kepler intubation system," *British journal of anaesthesia*, vol. 108, no. 6, pp. 1011–1016, 2012.

[8] G. A. Van Norman, "Drugs, devices, and the FDA: part 2: an overview of approval processes: FDA approval of medical devices," *JACC: Basic to Translational Science*, vol. 1, no. 4, pp. 277–287, 2016.

[9] R. Khurmi and J. Gupta, *Theory of machines*. Eurasia publishing house New Delhi, 2005.

[10] T. Yoshikawa, "Manipulability of robotic mechanisms," *The international journal of Robotics Research*, vol. 4, no. 2, pp. 3–9, 1985.

[11] D. Farhadi Machekposhti, N. Tolou, and J. Herder, "A review on compliant joints and rigid-body constant velocity universal joints toward the design of compliant homokinetic couplings," *Journal of Mechanical Design*, vol. 137, no. 3, 2015.

[12] J. L. Herder, "Energy-free systems. theory, conception and design of statically," Ph.D. dissertation, Delft University of Technology, 2001.

[13] G. A. Christiansson, "An experimental study of haptic feedback in a teleoperated assembly task," *Journal of Computing and Information Science in Engineering*, vol. 8, no. 4, 2008.

[14] T. Rahman, R. Ramanathan, R. Seliktar, and W. Harwin, "A simple technique to passively gravity-balance articulated mechanisms," *Journal of Mechanical Design, Transactions of the ASME*, 1995.

[15] S. Barros-Gomes, N. Orme, L. F. Nhola, C. Scott, K. Helfinstine, S. V. Pislaru, G. C. Kane, M. Singh, and P. A. Pellikka, "Characteristics and consequences of work-related musculoskeletal pain among cardiac sonographers compared with peer employees: a multisite cross-sectional study," *Journal of the American Society of Echocardiography*, vol. 32, no. 9, pp. 1138–1146, 2019.

[16] J. Carriere, J. Fong, T. Meyer, R. Sloboda, S. Husain, N. Usmani, and M. Tavakoli, "An admittance-controlled robotic assistant for semi-autonomous breast ultrasound scanning," in *2019 International Symposium on Medical Robotics (ISMR)*. IEEE, 2019, pp. 1–7.

[17] A. S. B. Mustafa, T. Ishii, Y. Matsunaga, R. Nakadate, H. Ishii, K. Ogawa, A. Saito, M. Sugawara, K. Niki, and A. Takanishi, "Development of robotic system for autonomous liver screening using ultrasound scanning device," in *2013 IEEE international conference on robotics and biomimetics (ROBIO)*. IEEE, 2013, pp. 804–809.

[18] S. G. Hart, "Nasa-task load index (nasa-tlx); 20 years later," in *Proceedings of the human factors and ergonomics society annual meeting*, vol. 50, no. 9. Sage publications Sage CA: Los Angeles, CA, 2006, pp. 904–908.

[19] J. K. Pickard, J. A. Carretero, and J.-P. Merlet, "Appropriate analysis of the four-bar linkage," *Mechanism and Machine Theory*, vol. 139, pp. 237–250, 2019.

[20] T. Yoshikawa, "Dynamic manipulability of robot manipulators," *Transactions of the Society of Instrument and Control Engineers*, vol. 21, no. 9, pp. 970–975, 1985.